

Excitonic enhancement of the Fermi-edge singularity in a dense two-dimensional electron gas

W. Chen, M. Fritze, W. Walecki, and A. V. Nurmikko

*Division of Engineering, Brown University, Providence, Rhode Island 02912
and Department of Physics, Brown University, Providence, Rhode Island 02912*

D. Ackley

Motorola Corporate Research, Phoenix, Arizona 85008

J. M. Hong and L. L. Chang

IBM Thomas J. Watson Research Laboratory, Yorktown Heights, New York 10598

(Received 8 October 1991)

We have investigated the interband recombination of dense two-dimensional (2D) electron gases in one-sided modulation-doped $\text{In}_x\text{Ga}_{1-x}\text{As}$ and GaAs asymmetric single quantum wells, under a near-resonance condition between an exciton level from a higher electronic subband and the Fermi level. Under such conditions, the excitonic resonant enhancement of the Fermi-edge singularity is clearly identified in both systems. The optical oscillator strength of the electrons at the Fermi level recombining with photoholes is enhanced by over two orders of magnitude through the resonant coupling with the exciton state. The strength and character of the interaction of the exciton with the 2D electron gas (~ 0.6 meV) is determined by photoluminescence spectroscopy, including its dependence on temperature and an in-plane magnetic field. In a perpendicular magnetic field, the periodic modulation in the formation of such coupled many-electron excitons leads to very large B^{-1} -periodic intensity oscillations in the photoluminescence.

I. INTRODUCTION

Interband optical spectroscopy has been widely applied to obtain important information on high mobility two-dimensional electron gases at semiconductor heterointerfaces, such as screening, electron exchange interactions, electron-impurity interactions, and electron-electron interactions.¹⁻³ Most recently, for example, optical signatures associated with the integer and fractional quantum Hall effects have been reported by several groups.^{4,5} The optical hole created by the photoexcitation is used as a probe of the physical properties of equilibrium electron systems. The creation of a photohole, however, also presents a finite perturbation to the equilibrium electron system and hence the study of the response of the electrons to the creation of the photohole, i.e. the many-electron-one-hole interaction in the presence of the Fermi sea, is of interest both in theory and experiment.^{6,7} This interaction was initially considered by Mahan⁸ for bulk semiconductors in the framework of the final-state electron-hole scattering. He showed that in spite of the static screening by the equilibrium electrons, an exciton-like effect still survives at moderate electron densities and there is a bound state slightly below Fermi level (recently called a Mahan exciton). This bound state results from the sharpness of the Fermi surface and the Pauli exclusion principle's restriction on the electron's scattering. Later theory included the dynamic response of the Fermi sea to the creation of the photohole, as well as the exchange effect due to the increased carrier density^{8,9} to show how the bound state eventually becomes unbound

and merges with the continuum. In optical absorption, a divergence of optical oscillator strength appears at a threshold energy (the Fermi level), giving rise to the term Fermi-edge singularity (FES), which persists into the high density limit and follows a power-law divergence.^{8,9} This many-electron excitonic feature is actually composed of two compensating processes, the scattering of electrons by the hole (vertex corrections) and the strong renormalization of the hole (self-energy effects).^{6,7,10}

Such a many-body enhancement is very sensitive to any broadening mechanisms such as the finite-hole mass, the lifetime contribution by the optical hole, and temperature.⁶⁻¹⁰ Any of these effects can broaden and even smear out the FES in both absorption and photoluminescence (PL).¹¹⁻¹⁴ In order to observe the FES experimentally (especially in PL) one must either keep the broadening at a minimum or enhance the interaction of the electrons at the Fermi level with the photohole. One example of the former case is found in Ref. 11 (in $\text{In}_x\text{Ga}_{1-x}\text{As}$ quantum wells), where the valence hole is localized by alloy potential fluctuations and we have practically an infinite-hole-mass situation, similar to the core-hole case in the soft x-ray problem. The latter case is the one which is the focus of this paper, where the scattering of the electrons at the Fermi level by the photohole is enhanced through the interaction with a near-resonant exciton.^{4,14}

The general design of the structures studied by us is shown in Fig. 1(a). It consists of a heterointerface (between layers *A* and *B*) with a back confinement layer (*C*), that is, a one-sided modulation-doped asymmetric single quantum well.¹⁵⁻¹⁹ The degenerate quasi-2D (where 2D

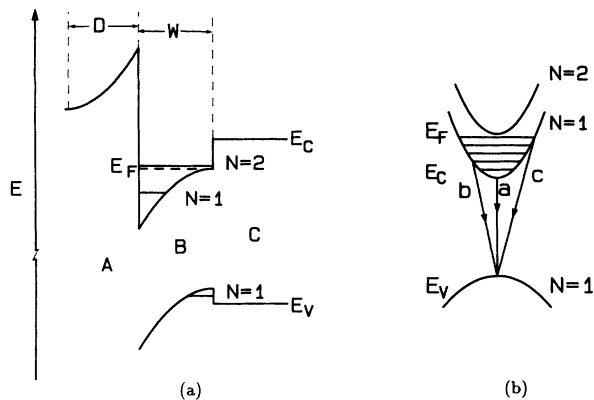


FIG. 1. (a) Schematic band diagram of the one-sided, modulation-doped, asymmetric single quantum well in the z direction. Note that the Fermi level (E_F) in the $N=1$ conduction subband is close (but below) the $N=2$ conduction subband. (b) Band diagram in k space (x - y plane), where processes a , b , and c represent the direct transitions, the impurity-assisted indirect transitions, and the resonant ($N=2$ exciton)-assisted transitions responsible for the excitonic enhancement of the FES, respectively.

denotes two-dimensional) electron gas fills the first electronic subband ($N=1$) up to the Fermi level E_F (being resident at interface A/B with wave function spread in z direction by typically about 60 \AA). The back confinement is useful for our purposes. First, it confines the optical hole at the opposite side of the quantum well so that the hole wave function substantially overlaps with the 2D electrons. Second, we make use of the next confined electric subband in the quantum well ($N=2$) whose energy is a few meV higher than the Fermi level in the $N=1$ subband and whose wave function in the z direction extends in the quantum well by approximately 150 \AA . A calculation performed by combining the static Poisson equation with the Schrödinger equation shows that the wavefunction overlap in the z direction between the $N=2$ subband and the $N=1$ hole level for our samples is typically a factor of 4–8 larger than that between the $N=1$ subband and the hole.²⁰ Note especially that the $N=2$ electric subband is not populated by equilibrium electrons in our case. This is the key condition which allows us to study the resonant coupling of the $N=2$ exciton with the FES in the $N=1$ subband and the interference between the two transitions using PL spectroscopy.

The $N=2$ exciton is a bound state of an electron in the $N=2$ subband and a photohole. Because the $N=2$ subband is (practically) empty in the case considered here, the exciton derived from this subband would not ordinarily experience the screening by the 2D equilibrium electron gas. Broadly speaking, however, because of its energetic proximity, the 2D electron gas in the $N=1$ subband induces a dipole moment of this exciton resulting in an interaction between them, as shown below, typically of energy $\sim 0.6 \text{ meV}$ at zero magnetic field. Ordinarily such interaction is small when compared with the Fermi energy and has no significant impact on the interband

recombination spectra, except when the energetic separation between the two transitions involving the $N=2$ exciton and the electrons at the Fermi level (FES) is comparable to this interaction (a few meV). Then the interband optical oscillator strength of the FES is then enhanced over two orders of magnitude through this resonant coupling with the $N=2$ exciton. The excitonic enhancement of the FES is very sensitive to temperature and it is broadened and typically smeared out by $T \sim 8 \text{ K}$ in our structures. The resonance condition can be tuned by an in-plane magnetic field or perpendicular electric fields; we have especially studied the continuous evolution of the excitonic enhancement of the FES using in-plane magnetic fields. In perpendicular magnetic fields, the interaction of the $N=2$ magnetoexciton with the Landau quantized 2D electrons is generally enhanced. Modified resonance behavior occurs where anticrossing and oscillator strength sharing are clearly identified as the highest occupied Landau level (LL) (the Fermi level resides in this LL) approaches the $N=2$ exciton. In perpendicular magnetic fields, the resonance condition between the FES and $N=2$ exciton is periodically modulated (with B^{-1} period) and very large PL intensity oscillations within the highest occupied LL are observed at low temperature, indicative of the periodic formation of the many-electron excitonic enhancement. The amplitude variations occur over three orders of magnitude and have been termed by us as “optical Shubnikov–de Haas oscillations (OSdH).”⁴

In terms of the possible radiative recombination processes in such systems, one must generally consider three different transitions. First involves the direct transitions of electrons and holes at the same k vector [process a in Fig. 1(b)].¹⁶ Second accounts for the impurity-assisted indirect transitions (process b).^{15,16,21} The third corresponds to the $N=2$ exciton-assisted FES induced by the resonant coupling of the two states (process c).^{7,22,6} It is this last key process that enables us to probe excitonic enhancement of the FES involving the electrons at k_F using PL spectroscopy,^{4,14} where the recombination processes mainly involve the thermalized photoholes at $k \approx 0$ at low temperature and low excitation level.

The remainder of this paper is organized as follows. In Sec. II we first summarize some general features of the PL spectra in our $\text{In}_x\text{Ga}_{1-x}\text{As}$ structures, including the role of impurity-assisted indirect transitions,^{16,23} the diagonal and off-diagonal transitions involving Landau levels, their temperature dependence, and the interaction with their magnetophonon sidebands.²⁴ We then focus our attention on the excitonic resonance enhancement of the FES in our $\text{In}_x\text{Ga}_{1-x}\text{As}$ structures. We characterize this resonant coupling of the FES with the $N=2$ exciton in terms of temperature dependence, the influence of an in-plane magnetic field,²⁵ and a simple empirical two-level model.²⁶ In perpendicular magnetic fields, we study the resonant coupling of the $N=2$ magnetoexciton with the highest occupied LL and investigate the periodic formation of the resonant enhancement of the FES involving this LL using both continuous-wave and time-resolved techniques. In Sec. III, we study the excitonic resonant enhancement of the FES in GaAs single quantum wells (QW's) by using similar techniques but also by including

electric-field tuning of the resonant interaction by a front-gate technique. The summary and conclusions are presented in Sec. IV.

II. OPTICAL SPECTROSCOPY OF $\text{In}_x\text{Ga}_{1-x}\text{As}$ ASYMMETRIC SINGLE QUANTUM WELLS

A. General spectroscopic properties

Photoluminescence measurements at low temperature were performed on series of samples placed in a superconducting magnet (fields up to 13.5 T) with a two-fiber arrangement providing optical access (one carrying the excitation and the other collecting the PL signals from the samples). The relevant parameters for three representative $\text{Al}_{0.15}\text{Ga}_{0.85}\text{As}/\text{In}_{0.15}\text{Ga}_{0.85}\text{As}/\text{GaAs}$ asymmetric-single-quantum-well samples (S1, S2, and S3) are listed in Table I [the layer geometry $A/B/C$ is defined in Fig. 1(a)] where W is the quantum-well width and D is the spacer layer thickness. The sheet densities (N_s) and the Fermi energies (E_F) in Table I were determined by Hall measurements. No signatures of the second conduction subband ($N=2$) being populated were found in Hall measurements in any of the three samples (including the study by Fourier transform of the details of SdH oscillations).

Figure 2(a) shows the low-temperature, low-excitation ($< 1 \text{ mW}/\text{cm}^2$) PL traces for the three samples at $B = 0 \text{ T}$ and $T = 2 \text{ K}$. As our convention, the long arrows indicate the spectral position of the $N=2$ exciton transition and short arrows indicate the spectral position of the FES. The quantity Δ denotes the energy separation between the two transitions. The low-energy peak denoted by E_0 in the figure involves the direct transition from the electrons at $k \sim 0$ in the $N=1$ conduction subband to the photoholes at $k \sim 0$. The $N=2$ exciton transition is

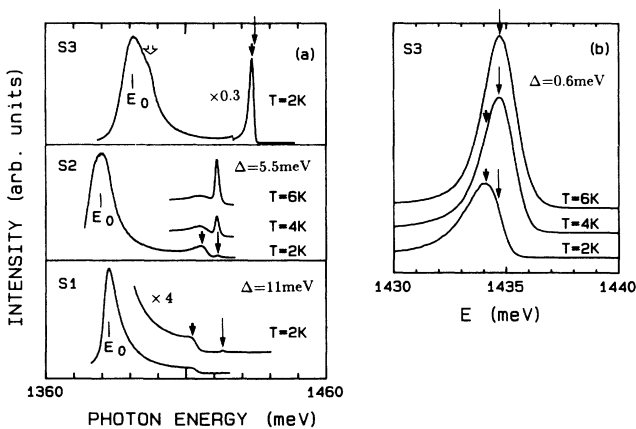


FIG. 2. (a) Low excitation-level PL spectra of three n -type $\text{In}_x\text{Ga}_{1-x}\text{As}$ SQW's, including the temperature dependence of the FES and $N=2$ exciton in sample No. S2. The short black arrow and the long arrow denote the spectral position of the FES and the $N=2$ exciton, respectively. The open arrow marks the phonon replica discussed in text. (b) The temperature dependence of the excitonic enhancement of FES in sample No. S3.

TABLE I. The relevant parameters for three representative $\text{Al}_{0.15}\text{Ga}_{0.85}\text{As}/\text{In}_{0.15}\text{Ga}_{0.85}\text{As}/\text{GaAs}$ asymmetric-single-quantum-well samples (S1, S2 and S3). Here D is the space layer thickness and W is the quantum-well width. The 2D electron Hall mobilities (μ), sheet densities (N_s), and Fermi energies (E_F) for the three samples listed in this table were determined by Hall measurements at $T = 2 \text{ K}$.

Sample	S1	S2	S3
D (\AA)	100	80	60
W (\AA)	150	150	150
μ ($\text{cm}^2/\text{V sec}$)	8.5×10^4	8×10^4	8×10^4
N_s (cm^{-2})	8×10^{11}	9.5×10^{11}	1.08×10^{12}
E_F (meV)	29.5	35	40.2

identified in the PL by raising the lattice temperature (to induce thermal population of the $N=2$ conduction subband) as well as in reflection spectra. For the sample No. S3 where the energy separation Δ is quite small, Fig. 2(b) shows the FES and $N=2$ region under higher spectral magnification. Additional justification for the particular placing of the arrows in Figs. 2(a) and 2(b) are given below. When comparing the PL and reflection spectra, no detectable Stokes shifts for the $N=2$ excitons are found in these samples. This reflects both the sample quality and the intrinsic nature of the $N=2$ exciton.

The sharp high-energy edge in the bottom PL trace in sample No. S1 [indicated by the short arrow in Fig. 2(a)] is the remnant of FES induced by the 2D electron gas in the $N=1$ subband without the influence of the $N=2$ exciton.^{4,14} The resonant channel for the excitonic enhancement of the FES is practically absent in this sample because of the larger energetic separation of the $N=2$ exciton and the Fermi edge ($\Delta \sim 11 \text{ meV}$ in this case). The direct Coulomb interaction between the 2D electrons in the $N=1$ subband and photoholes is significantly screened by the equilibrium electrons in the $N=1$ subband ($N_s \sim 10^{12} \text{ cm}^{-2}$) (Refs. 10 and 11) and further weakened by the reduced electron-hole wave-function overlap in the z direction,^{30,16} as displayed in our magnetoluminescence spectra, where the free-carrier-like electron-hole Landau-level transitions appear at $B \sim 1 \text{ T}$. In general, the FES in $\text{In}_x\text{Ga}_{1-x}\text{As}$ single QW's is significantly damped and broadened by the screened electron-hole interaction as well as by the finite in-plane light-hole mass ($m_h = 0.157m_0$, where m_0 is the free-electron mass). Because of the biaxial strain at the $\text{GaAs}/\text{In}_x\text{Ga}_{1-x}\text{As}$ interfaces in our structures, the in-plane heavy-hole bands ($\frac{3}{2}, \pm\frac{1}{2}$) are split off from the in-plane light-hole ($\frac{3}{2}, \pm\frac{3}{2}$) bands by about 60 meV .¹⁸ Only the latter is important in spectra such as in Fig. 2, given the low temperature of our experiments.

In sample No. S2, the value for the energy separation Δ is experimentally determined to be 5.5 meV and the PL trace now shows a clear excitonic enhancement of the FES at $T = 2 \text{ K}$. The enhancement is smeared out quickly with increasing temperature and disappears at $T \sim 8 \text{ K}$. In contrast, the $N=2$ exciton benefits from the thermally populated $N=2$ electrons and increases its intensity. For sample No. S3, a resonant condition is ob-

tained as $\Delta \sim 0.6$ meV and the PL trace shows a pronounced enhancement of FES, where the FES is now strongly coupled with the $N=2$ exciton state through the resonant interaction. The striking temperature dependence of the excitonic enhancement of the FES is shown in Fig. 2(b) with better spectral resolution. Note how the excitonic enhancement of the FES loses its strength quickly with increasing temperature. At 6 K, the spectrum is dominated by the thermally populated $N=2$ exciton recombination. There is an associated distinct change in the line shape from an asymmetric one at 2 K to a symmetric one at 6 K. Prior to analyzing the resonant enhancement of the FES and its dependence on the energy separation Δ in detail (Sec. II B), we first discuss some basic interband transition mechanisms involved in these observations.

In the PL traces for sample No. S 1 [Fig. 2(a)], the energy separation between the sharp high-energy edge (FES) and the low-energy peak (E_0) is 30 meV, in excellent agreement with the determination of E_F from the electron sheet density (N_S) in Table I. This agreement verifies that the sharp high-energy edge (FES) in the PL trace involves the electrons at the Fermi level $k = k_F$ and the holes at $k \approx 0$, an indirect transition in \mathbf{k} space.¹⁶ For the direct transition of the electrons and the holes at k_F , the high-energy spectral cutoff would occur at $(1 + m_e/m_h)E_F$ while the PL amplitude would start at a maximum value at the onset of the $N=1$ subband and decrease exponentially $\sim \exp[-(E - E_0)/k_B T]$ with increasing energy. This is clearly not observed here.

The scattering of the 2D electrons by the randomly placed impurities such as the ionized donors on the other side of the spacer layer and alloy fluctuation in the quantum well is chiefly responsible for the PL line shapes in the $\text{In}_x\text{Ga}_{1-x}\text{As}$ QW.¹⁶ The parallel \mathbf{k} vector (in the x - y plane) is no longer strictly a good quantum number of the 2D electron system with the presence of such scattering so that the electrons with $k \neq 0$ can recombine with the photohole at $k = 0$ with finite probability. The impurity and alloy potential scattering-assisted indirect transitions are higher-order effects and have generally much weaker oscillator strengths when compared with the direct transitions. However, at low temperature and low excitation level, the photoholes quickly relax to the top of the valence band with $k \sim 0$ and no holes are available at $k \approx k_F \sim 2 \times 10^6 \text{ cm}^{-1}$ for the direct recombination process. The net result is that the intensity of the indirect transition for electrons at finite wave vector is even stronger than those of the direct transition in PL spectra. As a consequence of scattering, the PL linewidth is broadened and the low-energy peak [E_0 in Fig. 2(a)] blueshifts from the actual onset of the $N=1$ subband by a small amount (e.g., ~ 1.2 meV for sample No. S2). The scattering potential of the 2D electron gas by the charged impurities (ionized donors on the other side of the spacer layer) depends on the thickness of the spacer layer. In the case of the sample with a thinner spacer layer (D), the E_0 peak is broader, as shown in Fig. 2(a) (compare the widths of the E_0 peaks for samples No. S1 and S2). The spectral blueshift ~ 1.2 meV is shown in Fig. 3 for sam-

ple No. S2, where the onset of the $N=1$ subband extrapolated from the Landau-level transitions is ~ 1.2 meV below the observed E_0 peak at zero magnetic field. We mention in passing that the usual perturbative approach to treating the dilute-impurity-scattering problem is to consider the \mathbf{k} vector a good quantum number in the zeroth order and include the scattering of electrons (or holes) by the impurity potential into virtual intermediate states before (after) the recombination in higher orders.¹⁶

In Fig. 2(a), the topmost trace for sample No. S3 also contains a shoulder within the E_0 feature as indicated by the open arrow. This shoulder appears about 36 meV below the Fermi-edge enhancement and is interpreted as being due to the participation by GaAs-like longitudinal-optical phonons (LO phonons) in the scattering processes of the electrons in the Fermi sea. The actual recombination process involves the LO-phonon-assisted indirect transitions and is indeed only found in our $\text{In}_x\text{Ga}_{1-x}\text{As}$ QW's with the Fermi energy $E_F \geq 36$ meV.^{18,24} Previous studies have argued that the hole-LO-phonon interaction, as evidenced by phonon sidebands in the exciton PL, should be screened out at sheet densities around $4 \times 10^{11} \text{ cm}^{-2}$, but LO phonons are also known to be important in the relaxation of hot electrons at high densities. In our case, the excitonic enhancement of the FES also promotes the phonon satellite appearing as the shoulder in Fig. 2(a).

Even though a pronounced spectral peak appears in the PL, indicative of strong resonant coupling between the $N=2$ exciton and enhancement of the FES associated with the 2D electron gas, our transport measurements showed no signature of the $N=2$ electric subband being populated. While the $N=2$ exciton level created by photoelectrons and photoholes is relevant in the optical process, such a charge neutral entity plays no role in transport measurements. This marks one major difference between optical and transport probes, in circumstances when the interaction between the electrons and photoholes is important.

In a perpendicular magnetic field, free electrons and holes are quantized into LL. Excepting the FES spectral region where the Coulomb effects are crucial, the commensurate LL spectral structure is very clear in our sample. As an example, Fig. 3 shows such magneto-PL spectra for sample No. S2 in the form of the familiar fan plot. The transition from the l th electron Landau level in the $N=1$ subband to the m th hole Landau level is denoted as $(l - m)$, where $l, m = 0, 1, 2, \dots$, respectively. The lines are a guide to the eye. The slopes are immediately expressed as

$$\frac{[E(B) - E(0)]}{B} = e\hbar \left[\frac{1}{2\mu} + \frac{l}{m_e} + \frac{m}{m_h} \right],$$

where μ is the reduced mass: $1/\mu = 1/m_e + 1/m_h$. The energy $E(0)$ is the extrapolated spectral position as the magnetic field approaches zero. The effective masses $m_e = 0.067m_0$ and $m_h = 0.159m_0$ thus obtained from Fig. 3 are consistent also with those for other samples. The dominant peaks in PL spectra at low temperature involve

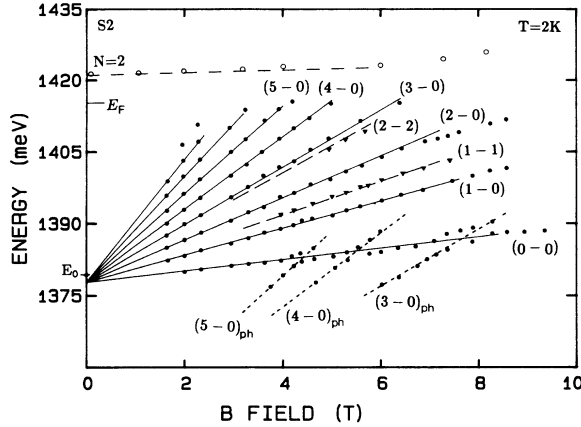


FIG. 3. The PL spectra in magnetic fields expressed as the fan plot for sample No. S2 at $T=2$ K. The straight lines are fitted through the data points.

the lowest hole Landau level, that is, the transition from successive electron Landau levels ($l=0, 1, 2, \dots$) to the lowest hole level ($m=0$), indicated by the solid lines and the filled circles in the figure. Except for the transition (0-0), all others are off-diagonal ($l \neq m$) transitions, induced by the impurity scattering in a magnetic field.¹⁶ The off-diagonal transitions are generally higher-order effects and have much weaker oscillator strengths when compared with the diagonal transitions ($l=m$). In analog to the zero-field case, because the photoholes only occupy the lowest Landau level at low temperature the off-diagonal transitions appear even stronger than the diagonal transition in our magnetoluminescence, as illustrated by the actual spectra in Fig. 4.

In the case of the sample with thinner spacer layer, the off-diagonal transitions become more pronounced. The left panel of Fig. 4 compares sample No. S2 ($D=80$ Å), for which the off-diagonal transitions (2-0) dominate over

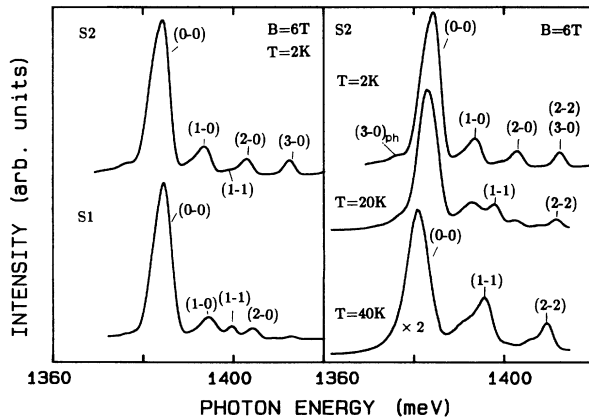


FIG. 4. Left panel: The influence of the spacer layer thickness on the relative intensity of the diagonal and off-diagonal LL transitions under similar experimental conditions ($D=80$ Å vs 100 Å). Right panel: the temperature dependence of the diagonal and off-diagonal transitions in sample No. S2.

the diagonal transitions (1-1) with sample No. S1 ($D=100$ Å) under the similar experimental conditions ($T=2$ K and $B=6$ T). The temperature dependence of the diagonal and the off-diagonal transitions for sample No. 2 are shown in the right panel of Fig. 4. The thermal population of the higher hole LL's ($m=1, 2$) is increased with increasing temperature. As a result, the intensity of the diagonal transitions also increases, becoming dominant in the PL spectra at $T=40$ K, as indicated by transitions (1-1) and (2-2) in Fig. 4.¹⁶ Although transitions (2-2) and (3-0) are nearly degenerate in our structures (Fig. 4) it is not difficult to separate them since they have quite different temperature dependences as shown. The different temperature dependences result from the distinct transition mechanisms involved in the two transitions. (The redshift of the entire spectrum at 40 K is due to the band-gap shrinkage while the Landau level spacings remain intact.)

As clearly seen in Fig. 3, the lowest interband LL transition (0-0) deviates from a straight line significantly for certain value of the magnetic field while additional peaks are also observed below this transition. We assign these low-energy PL emissions to the GaAs-like LO-phonon satellites associated with specific higher-lying Landau-level transitions, labeled as (4-0)_{ph}, (3-0)_{ph}, etc. in the figure, where the notation such as (4-0), (3-0) identifies the higher-lying parent transitions. The satellites extrapolate accurately to 36 meV below their parent Landau-level transitions as expected for GaAs LO phonons. Furthermore, distinct anticrossing behavior is seen in Fig. 3 of the phonon satellites with the (0-0) transition around the “crossing fields” of $B=4.5, 5.5,$ and 7.7 T in good agreement with the predicted “magnetophonon” resonance condition $l\hbar\omega_c = \hbar\omega_{LO}$ for $l=5, 4, 3$. When a particular satellite catches up with transition (0-0) near the crossing field, a resonant repulsion effect between the two transitions takes place as a result of the Fröhlich electron–optical-phonon interaction, reported recently in Ref. 24.

B. Excitonic enhancement of FES by the subband resonance condition: tuning in parallel magnetic fields

We have discussed some of the general features of photoluminescence spectra of the (In,Ga)As single quantum wells (SQW) structures above. We now return to the Fermi-edge singularity aspect of the problem in more detail and focus on its excitonic enhancement by the second subband proximity effect. The data of Fig. 2 already demonstrated clearly that as the energetic separation between E_F and the $N=2$ exciton is reduced, the PL intensity for electrons at the Fermi surface is subject to a very large enhancement factor. The interaction of the two relevant interband transitions, namely, the FES and the $N=2$ exciton state, is very roughly analogous to a familiar two-level resonance case where such interaction leads to mixing of the states.²⁶ Of course, the situation in the present case is considerably more complex because of the many-body aspect of the problem. Recently, the case presented by our experiments in zero magnetic field has

been analyzed by Muller *et al.*²² and by Hawrylak.⁶ Here we aim to present a very simple physical argument for intuitive purposes, based on the Fano-resonance ideas, in conjunction with additional experimental data obtained in parallel magnetic fields.

Experimentally we have employed a method of studying the details of this resonance coupling by the application of an in-plane magnetic field (an example of such fine tuning by an applied electric field is given in Sec. III). With the presence of a magnetic field up to 10 T parallel to the 2D electron (x - y) plane, no Landau-level quantization occurs in the density of states of the 2D electron system. The sheet density N_s of the 2D electron gas remains unchanged to first order (the finite hybridization of the electric and magnetic confinement causes a slight increase in the effective mass of the 2D electrons resulting in a small decrease in the Fermi energy).^{25,26,28} Note that the magnetic length ($l_B \approx 80$ Å) at 10 T is smaller than the $N=2$ exciton's Bohr radius ($a_x \approx 150$ Å) but still larger than the $N=1$ conduction subband wave-function spread in the z direction ($\Delta z \approx 60$ Å). The feature we take explicit advantage of is the fact that the $N=2$ exciton transition experiences a diamagnetic shift in an in-plane magnetic field, providing us an opportunity to fine-tune the resonance condition between the FES and $N=2$ exciton and observe the effects through PL. The diamagnetic shift for bulk excitons is proportional to B^2 , while the situation for the quasi-2D case has been analyzed both in the high- and low-field limits (Hasegawa and Eichler).³¹ For the 1S state considered here, we observe very little shift up to 4 T (blueshift of about 1 meV) while a nearly B^2 dependence is observed for higher fields (e.g., shift of ~ 4 meV from 6 to 10 T).

Representative PL spectra obtained in the presence of in-plane magnetic fields for sample No. S3 at $T=2$ K are shown in Fig. 5. As before, the short arrows indicate the excitonically enhanced FES while the long arrows indicate the spectral position of the $N=2$ exciton. In the left panel, the spectra show that the excitonic enhancement of the FES decreases quickly as we move the $N=2$ exciton away from the resonance (magnetic field increases from top to bottom). The intensity of the FES at 5 T is

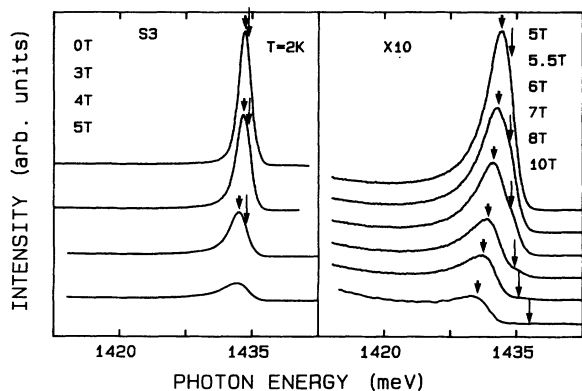


FIG. 5. The tuning of the excitonic enhancement of FES by an in-plane magnetic field at $T=2$ K (from $B=0$ T to $B=10$ T).

about six times less than that at zero field. Nonetheless, at 5 T, a significant excitonic enhancement of the FES is still present with the $N=2$ exciton state $\Delta=1.7$ meV away. In the right panel, we show the spectra from 5 up to 10 T. By about 10 T, the excitonic enhancement of the FES is barely visible, as the energy separation Δ has increased to 7 meV. We wish to emphasize that throughout this field range, recombination of electrons at E_F with the photoholes is the dominant feature in our spectra and the $N=2$ exciton itself is barely visible or invisible at $T=2$ K in PL. By raising the temperature to about 5 K (Fig. 6), however, we can observe the $N=2$ exciton transition and hence determine the energetic separation between the two transitions. The energy separation Δ for a set of in-plane fields has been measured to be as follows: $\Delta=0.6, 1.2, 2.5,$ and 4.2 for $B=0, 4, 6,$ and 8 T, respectively. As already described, the excitonic enhancement of the FES decreases rapidly with increasing temperature. This is illustrated in Fig. 6 for various in-plane magnetic fields (different Δ). The increase in the $N=2$ exciton amplitude at $T=5$ or 8 K (long arrows) is due to thermal population of the $N=2$ conduction band. The temperature dependence of the FES enhancement in turn reflects the coupling strength of the many-body interaction (see analysis below). The thermal smearing of the FES feature is expected since the activation energy ($\sim k_B T$) is expected to be comparable to the energy since the activation energy ($\sim k_B T$) is expected to be comparable to the energy of this many-electron interaction. In contrast to the value of about 30 K (Ref. 11) and 50 K (Ref. 12) we obtain a zero-field interaction energy of only ~ 8 K.

In our interpretation, the asymmetric line shape of the FES feature for $B > 5$ T (see, e.g., Fig. 5) is related with the hole recoil (finite mass), the impurity-induced level broadening and finite temperature effect. These damping and broadening factors temper the singular nature of the FES and cause the enhancement to be redistributed over

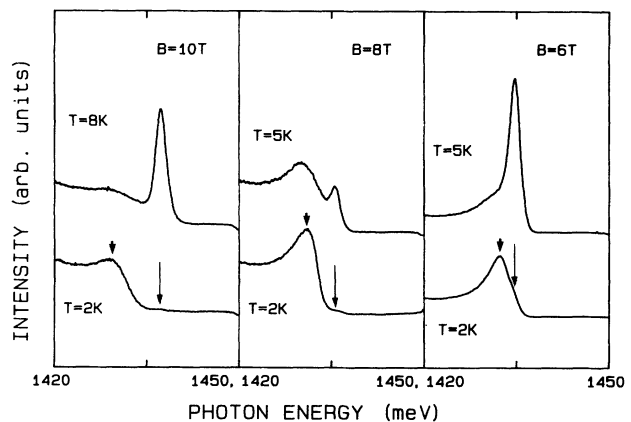


FIG. 6. Temperature dependence of the PL spectra for several in-plane magnetic fields ($B=6$ T, 8 T, and 10 T), also showing the quenching of the excitonic enhancement of FES and intensity buildup of the $N=2$ exciton with increasing temperature.

a finite width (3–4 meV) around the Fermi level. For $B < 5$ T, the linewidth decreases steadily with decreasing magnetic fields. At $B = 0$ T, a sharp resonance between the FES and $N = 2$ exciton results in a linewidth of 1.7 meV. Note again that no Landau-level structure is seen in Figs. 5 and 6 and in our discussion that we assume no field dependence in the screening properties of the 2D electrons in this case.

In Fig. 7, we plot the experimentally measured FES intensity enhancement factor in PL as a function of the energy separation Δ , together with results from the phenomenological model discussed next. It shows that the resonant coupling of the $N = 2$ exciton with the FES results in an enhancement of the oscillator strength of the FES more than a factor of 30. The experimentally obtained intensity enhancement factor P is measured by first subtracting the background signal (i.e., the PL intensity at the Fermi level without the influence of the $N = 2$ exciton, for example, at $B = 10$ T in Fig. 5) from the actual PL intensity (with the excitonic enhancement) and then normalizing it to this constant background. Thus we obtain, for example, values for the enhancement factor of $P = 26.2, 16.1,$ and 5.1 with the $N = 2$ exciton transition located $\Delta = 0.6, 0.9,$ and 1.7 meV away, respectively. The solid line is the theoretical fitting.

The physical model that we use here to demonstrate the resonant coupling of the $N = 2$ exciton with the FES is a nearly degenerate two-level model ($\Delta = E_2 - E_1$, where $\Delta/E_{1,2} \ll 1$), as shown in the inset of Fig. 7. The levels interact with each other through a perturbation V . The system is composed of N equilibrium electrons ($\mathbf{r}_1, \dots, \mathbf{r}_N$), a photoelectron, (\mathbf{r}_e) and a photohole (\mathbf{r}_h). We emphasize that we are not solving the many-body problem here (as done in Refs. 6, 7, and 22) but rather give a simplified physical interpretation of the Fano resonance aspect of the problem.²⁶

Before the interaction V is turned on, the system has two nearly degenerate eigenstates ϕ_1 and ϕ_2 . $\phi_1(\mathbf{r}_e, \mathbf{r}_h, \mathbf{r}_1, \dots, \mathbf{r}_N)$ is the many-body wave function representing the FES composed from the $N = 1$ conduc-

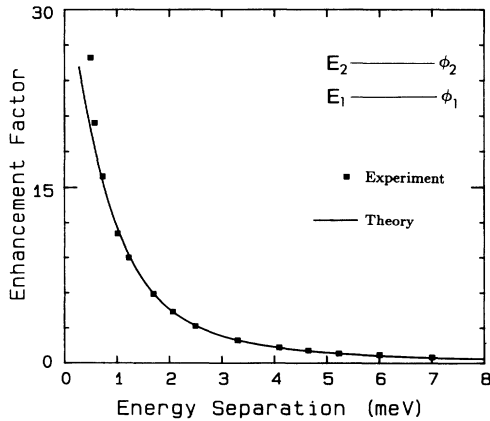


FIG. 7. The experimentally measured enhancement factor for the FES (filled squares) as a function of the energy separation (Δ) between the FES and the $N = 2$ exciton. The solid line is the theoretical fit according to the model discussed in text.

tion subband states (with the photoholes), without the influence of the $N = 2$ exciton and its energy is taken to be E_1 . The wave function ϕ_2 corresponds to the $N = 2$ exciton states formed by a photoelectron and a photohole pair and its energy is given by E_2 . Because the two states are decoupled with $V = 0$, the wave function ϕ_2 can be written as

$$\phi_2(\mathbf{r}_e, \mathbf{r}_h, \mathbf{r}_1, \dots, \mathbf{r}_N) = \Phi_2(\mathbf{r}_e, \mathbf{r}_h) \Phi_g(\mathbf{r}_1, \dots, \mathbf{r}_N), \quad (1)$$

where Φ_2 is the $N = 2$ exciton wave function and Φ_g is the ground-state many-body wave function of the 2D electron system.

The optical matrix element for ϕ_1 is

$$M_1 = \int \dots \int |\phi_1|^2 d\mathbf{r}_1 \dots d\mathbf{r}_N d\mathbf{r}_e d\mathbf{r}_h |_{\mathbf{r}_e - \mathbf{r}_h = 0}, \quad (2)$$

where M_1 is the oscillator strength of the FES in $N = 1$ subband without the influence of the $N = 2$ exciton.

The optical matrix element for ϕ_2 is

$$\begin{aligned} M_2 &= \int \dots \int |\phi_2|^2 d\mathbf{r}_1 \dots d\mathbf{r}_N d\mathbf{r}_e d\mathbf{r}_h |_{\mathbf{r}_e - \mathbf{r}_h = 0} \\ &= \int \int |\Phi_2|^2 d\mathbf{r}_e d\mathbf{r}_h |_{\mathbf{r}_e - \mathbf{r}_h = 0}. \end{aligned} \quad (3)$$

As the perturbation V is turned on, the FES state originating from in the $N = 1$ subband and the $N = 2$ exciton are coupled. Now we introduce ψ_1 and ψ_2 to represent the coupled wave functions for the FES and $N = 2$ exciton states, respectively. The interaction matrix elements are denoted by $V_{12} = V_{21}^* = \langle \phi_1 | V | \phi_2 \rangle$.

For the $N = 2$ exciton state, the coupled wave function is readily derived to be

$$\psi_2 = \sqrt{C} \left[\phi_2 + \frac{2V_{21}}{\Delta + \sqrt{\Delta^2 + 4|V_{12}|^2}} \phi_1 \right] \quad (4)$$

while the FES is given by

$$\psi_1 = \sqrt{C} \left[\phi_1 - \frac{2V_{12}}{\Delta + \sqrt{\Delta^2 + 4|V_{12}|^2}} \phi_2 \right], \quad (5)$$

where C is the normalization factor

$$C = \left[1 + \frac{4|V_{12}|^2}{(\Delta + \sqrt{\Delta^2 + 4|V_{12}|^2})^2} \right]^{-1}. \quad (6)$$

Since the coupled optical matrix element for the FES is given by

$$M'_1 = \int \dots \int |\psi_1|^2 d\mathbf{r}_e d\mathbf{r}_h d\mathbf{r}_1 \dots d\mathbf{r}_N |_{\mathbf{r}_e - \mathbf{r}_h = 0}. \quad (7)$$

We obtain for the FES enhancement factor $P = (M'_1 - M_1)/M_1$ that

$$P = \left[\frac{M_2}{M_1} - 1 \right] \frac{4|V_{12}|^2}{(\Delta + \sqrt{\Delta^2 + 4|V_{12}|^2})^2} C, \quad (8)$$

where M_1 is related to the unknown many-body wave function of the FES. In this model, we input the ratio M_2/M_1 experimentally from the data on sample No. S3. The optical matrix element of the $N = 2$ exciton (M_2) is six times as large as that of the direct transition of the

$N=1$ subband (E_0 transition in Fig. 2) for sample No. S3, because of the larger wave-function overlap between electrons and photoholes in the z direction [Fig. 1(a)]. The matrix element of the direct transition (E_0) in turn is 11 times as much as that of the FES without the influence of the $N=2$ exciton (M_1), as shown, for example, in Fig. 5 (in parallel field of $B=10$ T) and in Fig. 2. This fixes the ratio $M_2/M_1=66$ for sample No. S3.

In Fig. 7, the solid line shows the result of our model calculation with P as a function of Δ . The adjustable parameter V_{12} is chosen as 0.6 meV for the best fitting. This value hence represents the characteristic energy of the interaction of an exciton with 2D electrons in this particular $\text{In}_x\text{Ga}_{1-x}\text{As}$ SQW and is also in good quantitative agreement with the value deduced from our temperature-dependent measurements. (thermal breaking of the FES) In our analysis, we have overcome the difficulty in actually determining the FES wave function in the $N=1$ subband by resorting to direct experimental data. The discrepancy of our experimental data with the two-level model at small $\Delta \approx 0.6$ meV in Fig. 7 is possibly due to the resonant coupling of the $N=2$ exciton with the elementary excitations of the Fermi sea (beyond the rigid-Fermi-sea assumption)⁶ so that the experiment shows more pronounced enhancements than the model predicts.

C. Effect of perpendicular magnetic fields: optical Shubnikov de-Hass oscillations

In a perpendicular magnetic field, the 2D electron density of states is quantized and the Fermi level moves up and down into successive Landau levels (depopulation effect). In terms of the FES problem, this sweeping of the Fermi level results in the periodic formation (in $1/B$) of the Fano resonance condition with the $N=2$ exciton state. Here we briefly review and add further interpretation of this behavior which has been described in Ref. 4. Figure 8(a) shows the spectrally integrated PL intensity of the FES under such a periodic resonance condition at $T=2$ K. (Experimentally, we used a spectral-windowing approach in the vicinity of $N=2$ exciton transition to isolate the excitonically enhanced FES feature for its amplitude determination at $T=2$ K.) It shows sharp B^{-1} -periodic intensity oscillations with maximum-to-minimum amplitude ratio in excess of 1000:1 (OSdH). The maxima of the OSdH oscillations correlate with odd LL filling factors within 5% in the magnetic field range 3–10 T, while even filling factors are always located at the valleys of OSdH as illustrated in Fig. 8(b).⁴ We have pointed out that this correlation is related with the position of the electron Fermi level within the $N=1$ conduction subband (in localized or delocalized states), as well as the resonant aspect of the problem in terms of the $N=2$ exciton proximity effect.⁴ We now analyze the origin of the OSdH oscillations as follows.

In the low-field regime ($B \leq 1.7$ T), no clear oscillations are seen in the longitudinal resistance ρ_{xx} [Fig. 8(b)], yet the oscillations in OSdH remain quite distinct down to 1 T [Fig. 8(a)]. The delocalized states of successive LL's overlap significantly in this field range (1–1.7 T) and

since ρ_{xx} probes the spatially averaged density of states at the Fermi level across an entire sample it is difficult to discern Shubnikov-de Hass oscillations at such low fields. Above, we have already demonstrated how sensitive the resonant enhancement of the FES is to the energetic separation between the Fermi level and the $N=2$ exciton state. Thus the optical indicator (the OSdH oscillations) in this field range directly reflects the small “zig-zag” motion of the Fermi level. Note that the optical probe (OSdH) is not only used as an indicator of the density of states at the Fermi level but also of the precise energetic position of the Fermi level, whereas a transport probe (ρ_{xx}) is only sensitive to the density of the states at the Fermi level.

In strongly quantizing magnetic fields, even filling factors correspond to the Fermi energy being located in the gap between the LL's, i.e., in the localized states (spin degeneracy is not lifted in our field range), and the electron system is insulatorlike. As we have shown in this paper, the FES results from the repeated scattering of the electrons from the valence hole, and its oscillator strength depends on the number of available electrons at the Fermi surface which participate in the scattering as well as on the available phase space in the equal-energy shell for the electrons to be scattered into. This is how the oscillator

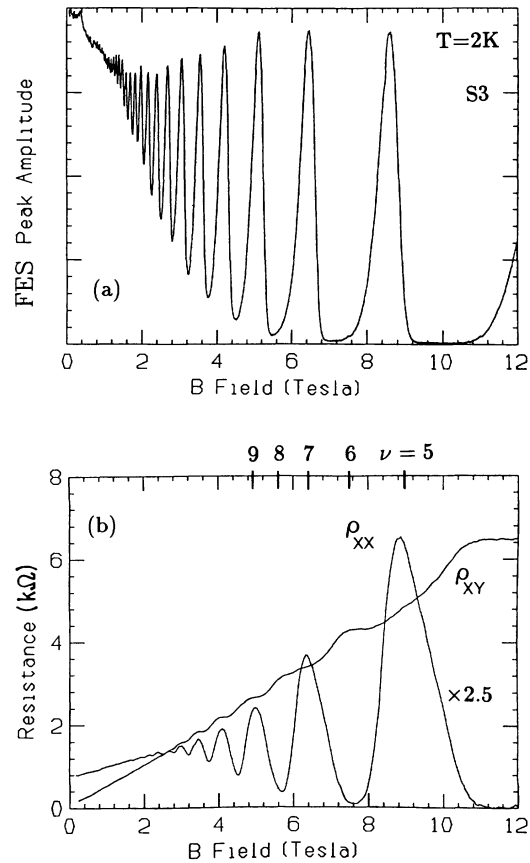


FIG. 8. (a) Variations in the PL amplitude corresponding to the excitonic enhancement of FES in sample No. S3 as a function of perpendicular magnetic field at $T=2$ K; (b) Hall data on the same sample.

strength of the FES depends on the density of states at the Fermi energy. More detailed theoretical calculations remain challenging in quantizing magnetic fields of this problem,^{6,23} although we note recent initial work by Hawrylak on this subject.⁶ Qualitatively, however, we argue that the FES should be suppressed when the E_F is located in the localized states. This is in agreement with our experimental findings, that is, a pronounced enhancement of the FES is present only when E_F lies within the extended states. In addition, the resonant coupling of the $N=2$ exciton with the approaching LL is the key mechanism responsible for the resonant enhancement of the FES in our case of the second subband proximity effect and it requires the resonance condition between the $N=2$ exciton and the nearest interacting LL. Hence, in order to observe the pronounced magnetic-field driven excitonic enhancement such as in Fig. 8(a), we need these two conditions both being satisfied. The near-resonance aspect with the $N=2$ exciton explains why the effective magnetic-field width of our OSdH oscillations [Fig. 8(a)] are even sharper than the corresponding peaks of ρ_{xx} in Hall measurements [Fig. 8(b)]. To observe very pronounced intensity maxima in the OSdH measurements requires that the two conditions are met, while the observation of the ρ_{xx} maxima only requires the condition that the Fermi level be located in the extended states. For example, because the $N=2$ exciton in sample No. S3 is initially in very near resonance with the Fermi level at zero field, and undergoes much smaller diamagnetic shifts in magnetic fields compared with the Landau levels, the two conditions are in this particular case preserved well in magnetic fields up to 9 T. As a result, we can observe pronounced intensity oscillations whose maxima correlate well with odd filling factors.

When the two conditions are not satisfied, the OSdH oscillations become much less pronounced. We have seen much smaller and broader oscillations in other samples with the Fermi level 3–7 meV below the $N=2$ exciton states in zero field. The maxima-to-minimum excursions of the oscillations are in the range of 2 to 6 with broad linewidths. Furthermore, the maxima of the oscillations do not correlate well with odd filling factors.

An illustration of the relevant interactions in perpendicular fields is shown in Fig. 9 which displays the PL spectra involving the $N=2$ exciton and the highest occupied LL (3-0) at $T=1.8$ and 8 K. The magnetic-field range ($B=7.6$ – 8.4 T) corresponds to the initial intensity buildup within one period of an OSdH oscillation (full amplitude excursion from $B=7.3$ to $B=9.5$ T). The spectra at $T=1.8$ K show that the intensity of LL transition (3-0) (not the $N=2$ exciton) is very much enhanced and it starts to deviate from its linear energy shift with magnetic field as it approaches the $N=2$ exciton states (whose position indicated by the long arrows). This intensity enhancement of the highest LL transition by the exciton resonance is very sensitive to temperature and becomes much less pronounced at $T=8$ K, as shown in the right panel of Fig. 9. In an opposite sense, the intensity of the $N=2$ exciton transition increases at $T=8$ K as the LL approaches this state. As before, the $N=2$ exciton is practically undetectable in PL at $T=1.8$ K and its spec-

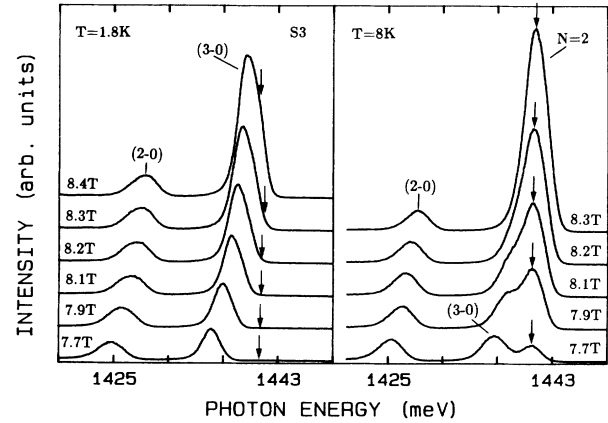


FIG. 9. Photoluminescence spectra within one period of the OSdH oscillations at two different temperatures for sample No. S3, showing the intensity buildup of the resonant excitonic enhancement in the highest occupied LL (3-0) at $T=1.8$ K (left panel). The right panel highlights role of the thermally populated $N=2$ subband at $T=8$ K, as this LL approaches the resonance with the $N=2$ exciton state.

tral position can only be determined from higher temperature data. In analog to the zero-field case, the increase of the $N=2$ exciton intensity results from the thermally activated electrons which are supplied by the approaching LL. The “anticrossing” behavior of the approaching LL is much reduced at $T=8$ K, compared with that at $T=1.8$ K. No anticrossing behavior is observed at $T=20$ K where the approaching LL simply continues to shift linearly with magnetic field becoming eventually overwhelmed by the $N=2$ exciton at $T=20$ K.

As a further means of characterizing some of the kinetics of the coupled many-electron excitations, we have employed time-resolved photoluminescence spectroscopy to determine the lifetime (from the PL decay) of the $N=2$ exciton, the FES-($N=2$ exciton) complex as well as transitions involving free electrons deeper in the $N=1$ subband in magnetic fields. The excitation source was a synchronously pumped DCM dye laser (pulse width < 7 ps). The detection system was based on a streak camera equipped with CCD readout, with the system time resolution of 10 ps. The samples were placed in our high-field superconducting magnet, this time with windows providing the optical access to eliminate the temporal broadening of the optical pulses induced in the fiber coupling approach. Here, we summarize some of the salient features of these results.

The left-hand panel of Fig. 10 compares the lifetime data for the following three PL transitions for sample No. S3 at $T=2$ K: the lowest LL (0-0) evolving from the E_0 transition, the FES-($N=2$ exciton) feature [measured at specific values of magnetic field where the resonance occurs, corresponding to the intensity maxima of OSdH oscillations in Fig. 8(a)], and the $N=2$ exciton state. In zero field, the E_0 transition and the FES-($N=2$ exciton) feature have lifetimes of 980 ± 15 ps and 680 ± 15 ps, respectively. The pure $N=2$ excitons (detectable at the magnetic fields corresponding to the valleys in the OSdH

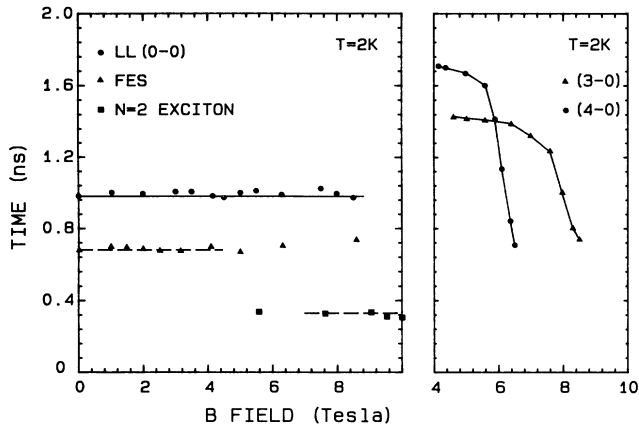


FIG. 10. (a) The lifetime of the lowest LL transition (0-0), of the resonant feature of FES and $N=2$ exciton [FES-($N=2$ exciton)] and the $N=2$ exciton in perpendicular magnetic fields at $T=2$ K for sample No. S3 from the time-resolved PL. (b) The lifetime of the two LL transitions (3-0) and (4-0) as they approach the resonance with the $N=2$ exciton to form the FES-($N=2$ exciton) complex in perpendicular magnetic fields. The solid and dashed lines are a guide to the eye.

oscillations) decayed typically much faster, with a lifetime of ~ 350 ps in our $\text{In}_x\text{Ga}_{1-x}\text{As}$ structures quite generally (due to the large electron-hole wave-function overlap). Up to the maximum field of 10 T in these experiments, very little change was observed in the lifetime of these transitions. This is especially striking, given the very large excursions in the amplitude of the FES luminescence (OSdH oscillations) and points directly to an interpretation in which the formation probability, not the lifetime, of the FES-($N=2$ exciton) complex establishes the key controlling kinetic step in the overall process. The measurements of the risetime in the transient PL spectroscopy were, unfortunately, beyond the present temporal resolution of the system. In a rate equation concept, the formation rate of the FES-($N=2$ exciton complex) depends on the availability of the $N=2$ exciton to polarize the 2D electron gas when compared with other channels. For example, given a magnetic-field value for which E_F lies within the localized states of the LL spectrum would intuitively correspond to a circumstance where the FES formation rate is lessened. Further time-resolved studies of this problem are presently under way.

The transient spectroscopy does, however, give us some direct insight about the nature of the state mixing which occurs when nearby LL transitions begin to approach the FES resonance region. This is illustrated in the right-hand panel of Fig. 10, which shows the reduction in the lifetime of the (3-0) transition (filled triangles) decreasing from approximately 1.4 ns at 5.6 T (where the separation in energy from this LL to the $N=2$ exciton transition is about 11 meV) to a value consistent with that of the hybridizing FES-($N=2$ exciton) transition. Note that the shortening in the LL lifetime occurs rather abruptly, dropping from about 1.24 ns at $B=7.7$ T to 740 ps at $B=8.6$ T (the corresponding spectral changes were already highlighted in Fig. 9). This decrease is consistent with the increase in the optical oscillator strength

due to the resonant coupling process. Similar behavior was observed for transition (4-0) in the magnetic-field range ($B=5.5$ – 6.5 T) in the right-hand panel of Fig. 10 where its lifetime is indicated by the filled circles. This LL transition has a lifetime of about 1.7 ns at $B=4$ T where it is located about 9 meV below the $N=2$ exciton. As it moves closer into resonance with the $N=2$ exciton, the formation of the resonant enhancement of the FES in this LL transition again leads to distinctly shorter lifetime (710 ps at $B=6.5$ T).

III. EXCITONIC ENHANCEMENT OF THE FES IN ASYMMETRIC GaAs SINGLE QUANTUM WELLS

The structures used in this portion of our work were $\text{Ga}_{0.7}\text{Al}_{0.3}\text{As}/\text{GaAs}/\text{Ga}_{0.85}\text{Al}_{0.15}\text{As}$ [$A/B/C$ in Fig. 1(a)] modulation-doped asymmetric single quantum wells, with spacer layer thicknesses (D) and quantum-well widths (W) again used as adjustable parameters. Some of this work has been recently reported by us¹⁴ and is expanded here further. The degenerate 2D electron subband ($N=1$) is formed at the $\text{Ga}_{0.7}\text{Al}_{0.3}\text{As}/\text{GaAs}$ heterointerface with Fermi energies E_F ranging from 15 to 40 meV in our samples. The back confinement is provided by a 300 Å thick $\text{Ga}_{0.85}\text{Al}_{0.15}\text{As}$ layer of and the wave function of the $N=2$ electric subband extends across the GaAs quantum well ($W=150$ – 250 Å). Similar to the $\text{In}_x\text{Ga}_{1-x}\text{As}$ structures discussed above, the E_F is adjusted by our sample designs to lie a few meV below the $N=2$ subband while taking special care to ensure that the $N=2$ subband is empty. The electrons' mobility at $T=4$ K is about 2 – 3×10^5 cm^2/Vs (\sim three times higher than in the $\text{In}_x\text{Ga}_{1-x}\text{As}$ systems).

Figure 11 shows a portion of the PL spectra recorded from three samples at $T=0.4$ K. The spectral range corresponds to the transitions involving the electrons occupying phase space in the vicinity of the Fermi level and

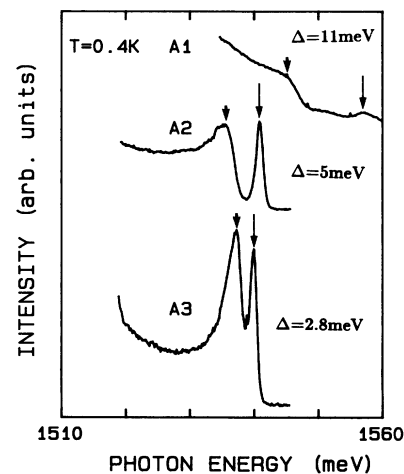


FIG. 11. Photoluminescence spectra from three n -type GaAs SQW's in the region of the $N=2$ exciton (long arrow) and FES (short arrow) at $T=0.4$ K, showing the amplitude enhancement of the FES for different values of the energy separation Δ .

the $N=2$ subband with photoholes in the $N=1$ valence subband. As a consequence of reduced impurity and alloy scattering (vs $\text{In}_x\text{Ga}_{1-x}\text{As}$), as well as the low temperature, we can now clearly observe a spectrally distinct FES feature (short arrows) as well as the $N=2$ exciton (long arrow). We mention in passing that the samples were placed in a ^3He refrigerator in a superconducting magnet with a two-fiber array setup for excitation and collection of the PL signals. The spacer layer thickness, the sheet density, and the quantum-well width are 60 \AA , $1.06 \times 10^{12} \text{ cm}^{-2}$, and 150 \AA , respectively, for sample No. A1, and 80 \AA , $0.91 \times 10^{12} \text{ cm}^{-2}$, and 200 \AA , respectively, for sample No. A3. The parameters for sample No. A2 are only slightly different from those for sample No. A3 as described below. The three traces show a clear trend of the evolution of the subband resonance enhancement of the FES as the $N=2$ exciton state approaches the Fermi level. In sample No. A1, the energy separation is relatively large ($\Delta=11 \text{ meV}$) and the PL trace shows a high-energy spectral edge at the Fermi level, i.e., a remnant of the FES from the $N=1$ subband, without the influence of the $N=2$ exciton. The middle trace (sample No. A2) shows a distinct excitonic enhancement of the FES under conditions where $\Delta=5 \text{ meV}$. A very striking, spectrally sharp excitonic enhancement of the FES is seen in the bottom trace for sample No. A3 where Δ has decreased to 2.8 meV . We mention in passing that in our structures, the recombination from the GaAs buffer layer ($\sim 1513 \text{ meV}$) strongly interferes with the PL at the $N=1$ subband edge ($\sim 1510 \text{ meV}$). Generally, the PL intensity from the buffer layer is ~ 100 times stronger than that involving the $N=1$ electric subband and the valence hole subband. Fortunately no such difficulties occur in the important spectral window near the $N=2$ transition.

The $N=2$ exciton viewed through PL shows no detectable Stokes shift at low temperature with respect to its measured absorptive resonance. We have also examined other samples with larger quantum-well widths ($W \geq 250 \text{ \AA}$), in which the $N=2$ excitons in PL become "extrinsic" and $2\text{--}3 \text{ meV}$ Stokes shifts were observed. In such a circumstance, the weakly localized $N=2$ excitons are not interacting with the 2D electron gas as efficiently as in the case highlighted here. For example, no distinct excitonic enhancement of the FES was observed for a sample with electron mobility $\sim 4 \times 10^4 \text{ cm}^2/\text{Vs}$ and an extrinsic $N=2$ exciton (2-meV Stokes shift) even though the Fermi level in this case was located only 3 meV away from the $N=2$ exciton, the latter dominating the PL signal.

The optimization of the excitonic enhancement of the FES such as in Fig. 11 calls for detailed sample designs which give consideration for such as the relative wavefunction overlaps of the $N=1$ and 2 conduction subbands with the valence hole, a relative high mobility of the 2D electron gas, an appropriate quantum-well width (e.g., comparable with the exciton's Bohr radius), a suitable spacer layer thickness, and good heterointerfaces (no traps or dislocations). We note that other designs with rich conduction subband structure such as wide parabolic wells²⁹ and the quasi-1D electron system²⁷ are also attractive for the study of the subband resonance enhancement effect on the FES. For example, we have found that in a

wide (Al,Ga)As parabolic well, the closely spaced electronic subbands ($\sim 1 \text{ meV}$) act as resonant channels to enhance and redistribute to FES across the entire shallow Fermi sea.²⁹

In the remainder of this section, we focus on the study of the excitonic enhancement of the FES in sample No. A3. This is done while keeping in mind the physical ideas and interpretation discussed in Sec. II for the (In,Ga)As structures. As the bottom PL trace of Fig. 11 shows, the resonant excitonic enhancement of the FES builds up substantially and emerges as a distinct peak at the spectral position of the Fermi level. This enhancement is very sensitive to temperature, as shown in Fig. 12,¹⁴ so that the FES is heavily attenuated by $T \sim 8 \text{ K}$, beyond which the spectrum is dominated by the $N=2$ exciton transition involving the electrons which are thermally activated to the $N=2$ subband. This temperature dependence is quite similar to that observed in our $\text{In}_x\text{Ga}_{1-x}\text{As}$ structures for the FES feature (e.g., sample No. S3 and S2 above). The activation energy of the FES deduced from this temperature dependence ($\sim 0.7 \text{ meV}$) is indeed nearly identical to that observed, e.g., for the (In,Ga)As sample No. S3. This directly strongly supports the notion that the excitonic enhancement of the FES is an intrinsic optical property of the 2D electron system, independent of the host material.

We have also performed in-plane magnetic-field measurements on sample No. A3 to detune the initial near-resonance condition between the $N=2$ exciton state and the FES. The spectra recorded at various in-plane magnetic fields are shown in Fig. 13. As the $N=2$ exciton is diamagnetically tuned away from the resonance, the excitonic enhancement of the FES decreases rapidly. For $B \approx 10 \text{ T}$, the remnant of the FES has evolved into a step-like high-energy edge. The resonant nature of the excitonic enhancement of the FES in the sample is hence clearly identified by using in-plane magnetic fields. Following the phenomenological model developed in Sec. II and the fitting procedure which led to Fig. 7 above, the

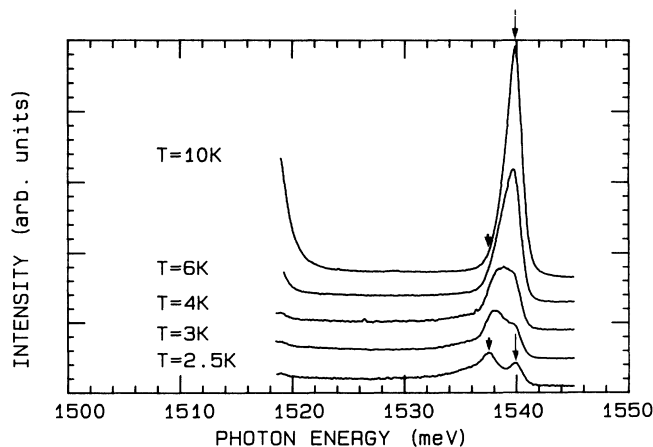


FIG. 12. Temperature dependence of the PL spectrum showing the quenching of the FES emission and the buildup of the $N=2$ exciton from the thermal excitation of electrons into the $N=2$ subband.

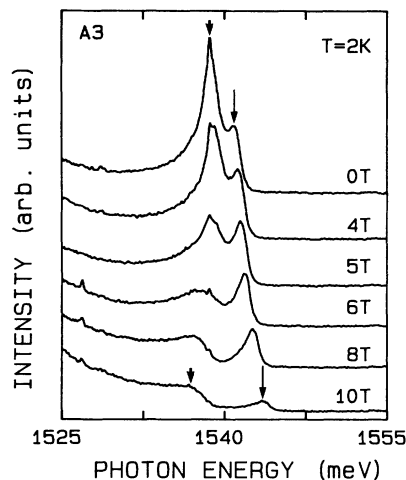


FIG. 13. The effect of an in-plane magnetic field on the FES (from tuning of Δ) in sample No. A3 at $T=2$ K.

coupling matrix element (V_{12}) is deduced as 0.7 meV in sample No. A3. This in turn is again in good agreement with our temperature dependence measurement (Fig. 12).

As another method of fine-tuning the resonance condition, a perpendicular external electric field was applied to sample No. A3 through a top Schottky gate. Note the difference between the application of the in-plane magnetic field and such a front gate. The role of the former is to move the $N=2$ exciton state to higher energies (diamagnetic shift), while the sheet density (N_s) and the Fermi energy remains unchanged to first order. In the latter case, the sheet density and the Fermi energy of the 2D electron gas are altered by varying the gate voltage as electrons are depleted or accumulated at the GaAs/Ga_xAl_{1-x}As heterointerface. A practical difficulty in our structures was the presence of only a thin undoped GaAs cap layer (400 Å) so that the sheet density immediately decreased by $\sim 30\%$ when a semitransparent gate (Ni-Cr) was evaporated directly on the surface of the sample. To avoid this initial depletion, we placed a thin layer of insulating photoresist (~ 1000 Å) on the sample surface as a buffer layer on which a 300-Å layer of Ni-Cr alloy was evaporated. By applying a forward bias to the metal gate we increase the sheet density of 2D electrons and move the Fermi level closer to the $N=2$ exciton. The PL spectra with different gate voltages for sample No. A3 are shown in Fig. 14. As can be seen, the resonant excitonic enhancement at the FES is increased with increasing sheet density (N_s) and eventually dominates over the $N=2$ exciton.

As already discussed for the In_xGa_{1-x}As structures, in the presence of a perpendicular magnetic field, the 2D electron gas is quantized into Landau levels and the Fermi level undergoes the zigzag motion with successively depopulated LL's. Hence, the resonant excitonic enhancement of the FES is modulated in magnetic fields, giving rise to the pronounced B^{-1} -periodic oscillations in its amplitude, as recorded in Fig. 15 for sample No. A3 at four different temperatures (the OSdH oscillations).¹⁴ In

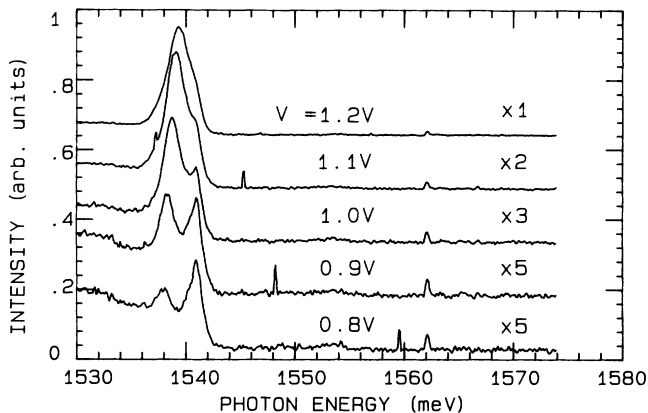


FIG. 14. Variation in the FES amplitude from tuning of Δ by an applied voltage on a gated sample No. A3 at $T=2$ K.

Fig. 15, the oscillations in the low-field region ($B < 3$ T) disappear at 10 K. This is consistent with our temperature data at $B=0$ T, where we show an activation energy of 8 K. However, the oscillations in the high-field region ($B > 4$ T) still persist at 10 K, but are quickly washed out in the temperature range of 15–20 K, as shown in the figure. The background signal PL at $T=20$ K is due to the thermally activated $N=2$ exciton, which now dominates the PL. The activation energy estimated by us from the temperature dependence of OSdH is ~ 1.6 meV (18 K) for $B \geq 4$ T, that is, a factor of 2.2 larger than in zero field.

Selected examples of actual PL spectra in magnetic fields ($B=6.8-7.1$ T) at $T=0.4$ K are displayed in Fig. 16. This field range corresponds to one cycle in the OSdH oscillations. The resonant excitonic enhancement in the oscillator strength for the highest occupied LL is unambiguously identified in Fig. 16, which shows that the PL intensity of the highest occupied LL ($l=3$) increases quickly and eventually towers over the $N=2$ exciton at

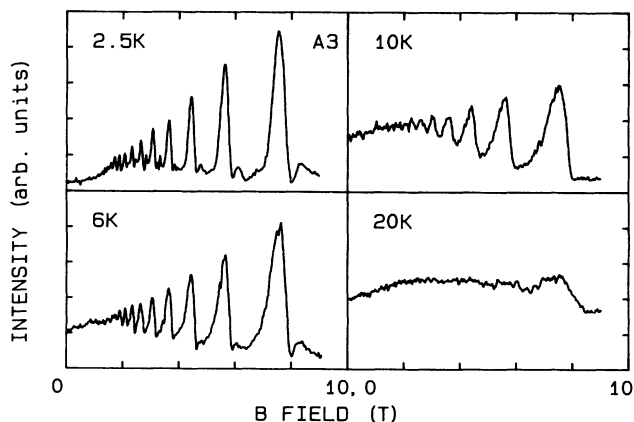


FIG. 15. The PL intensity variations (of the resonant enhancement of FES) as a function of perpendicular magnetic field (OSdH oscillations) at $T=2.5, 6, 10,$ and 20 K. The background PL signal at $T=20$ K is due to the thermally populated $N=2$ exciton.

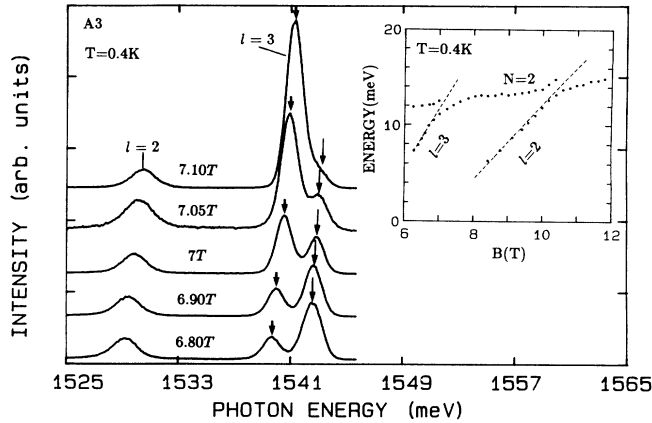


FIG. 16. Details of the PL spectra within one period of the OSdH oscillations at $T=0.4$ K, showing the strong enhancement of the oscillator strength in the highest occupied LL transition ($l=3$) as this LL approaches the $N=2$ exciton state. Inset: the spectral positions of the LL transitions ($l=3$), ($l=2$), and the $N=2$ exciton as a function of magnetic field at $T=0.4$ K, showing the anticrossing of the two LL transitions with the $N=2$ exciton (the dashed lines indicate the linear spectral shifts of the two LL transitions with magnetic field at $T=20$ K).

$T=0.4$ K, as this LL approaches the resonance condition with the $N=2$ exciton state. The interaction between the $N=2$ exciton and the nearly resonant LL (note that the Fermi level resides in this LL), is responsible for the mixing of the oscillator strength of the two transitions, similar to the case that we have already modelled in zero field in Sec. II B. In the inset of Fig. 16, we have recorded the spectral position of the two transitions as a function of magnetic field at $T=0.4$ K. As shown, the Landau level ($l=3$) begins to deviate from its linear shift with magnetic field (indicated by the dash line) in this field range and switches its “Landau-level” character to the “exciton” character as it approaches the $N=2$ exciton resonance, with the already described changes in its optical oscillator strength. The inset of Fig. 16 gives us yet another measure of the energy scale of this interaction which can be estimated from the anticrossings to be ~ 1.5 meV at $B \sim 7.5$ T and ~ 1.8 meV at $B \sim 11$ T. These values are consistent with our activation measurements, e.g., from the temperature dependence of the OSdH in Fig. 15. The oscillator strength mixing and the anticrossing behavior as demonstrated in Fig. 16 are also very sensitive to temperature. By $T \approx 20$ K, no PL intensity enhancement and anticrossing behavior of the approaching LL (e.g., $l=3$) is observed [that is, the LL

($l=3$) follows the dash line in the inset of Fig. 16, shifting linearly with magnetic field]. This again is similar to the behavior observed in (In,Ga)As sample No. S3.

IV. SUMMARY

We have investigated the interband recombination of a dense 2D electron gas formed in $\text{In}_x\text{Ga}_{1-x}\text{As}$ and GaAs-based one-sided modulation-doped asymmetric single quantum wells, under a near-resonance condition between the Fermi-edge singularity, originating from the first conduction subband, and the $N=2$ exciton states. Due to an energetic proximity typically of a few meV, the resonant coupling between the two transitions results in an excitonic enhancement of the FES over two orders of magnitude. We have studied the temperature dependence of this enhancement of the FES by using an in-plane magnetic field, and determined the interaction matrix element (typically ~ 0.6 meV) between the $N=2$ exciton states and 2D electron gas. We have demonstrated through a simple phenomenological two-level model the nature of the resonant coupling of these two states and their mixing and interference. In a perpendicular magnetic field, we have characterized the resonant coupling of the $N=2$ exciton with the adjacent highest occupied LL’s and observed the excitonic enhancement to the approaching LL at low temperature ($T \leq 2$ K) in both the $\text{In}_x\text{Ga}_{1-x}\text{As}$ and GaAs systems. We have employed transient PL spectroscopy to determine the radiative lifetime of various transitions to show that the formation of the FES-($N=2$ exciton) complex, not its decay, is the critical kinetic step. Finally, we have shown how the periodic formation of the excitonic resonant enhancements of the FES in the highest occupied Landau level in a perpendicular magnetic field leads to very large B^{-1} -periodic intensity oscillations in PL at low temperature with excursions over two orders of magnitude and conditions under which these oscillations are commensurate with those in the longitudinal Hall resistance in the quantum Hall regime.

ACKNOWLEDGMENTS

The authors thank P. Hawrylak and S. Schmitt-Rink for useful discussions. We are grateful to B. Brandt and Don Heiman in National Magnet Laboratory at MIT for the expert advice on the ^3He refrigerator. We authors also thank B. B. Goldberg for the advice on Hall measurements and G. Vecris for his interest. The research at Brown University was supported by the National Science Foundation (DMR-9112329) and in part by IBM. The work at IBM is partly sponsored by the Army Research Office.

¹B. B. Goldberg, D. Heiman, and A. Pinczuk, Phys. Rev. Lett. **63**, 1102 (1989).

²A. Pinczuk, S. Schmitt-Rink, G. Danan, J. P. Valladares, L. N. Pfeiffer, and K. W. West, Phys. Rev. Lett. **63**, 1633 (1989).

³M. Potemski, R. Stepniowski, J. C. Maan, G. Martinez, P.

Wyder, and B. Etienne, Phys. Rev. Lett. **66**, 2239 (1991).

⁴W. Chen, M. Fritze, A. V. Nurmikko, D. Ackley, C. Colvard, and H. Lee, Phys. Rev. Lett. **64**, 2434 (1990).

⁵B. B. Goldberg, D. Heiman, A. Pinczuk, L. Pfeiffer, and K. West, Phys. Rev. Lett. **65**, 641 (1990); H. Buhmann, W. Joss,

- K. von Klitzing, I. V. Kukushkin, G. Martinez, A. S. Plaut, K. Ploog, and V. B. Timofeev, *ibid.* **65**, 641 (1990); A. J. Turberfield, S. R. Haynes, P. A. Wright, R. A. Ford, R. G. Clark, J. F. Ryan, J. J. Harris, and C. T. Foxon, *ibid.* **65**, 637 (1990).
- ⁶P. Hawrylak, Phys. Rev. B **42**, 8986 (1990); **44**, 6262 (1991); P. Hawrylak (unpublished).
- ⁷A. E. Ruckenstein and S. Schmitt-Rink, Phys. Rev. B **35**, 7551 (1987); J. F. Mueller, A. Ruckenstein, and S. Schmitt-Rink, Mod. Phys. Lett. B **2**, 135 (1991).
- ⁸G. D. Mahan, Phys. Rev. **163**, 163 (1967); **153**, 153 (1967).
- ⁹P. Nozières and C. T. De Dominicis, Phys. Rev. **178**, 1097 (1969).
- ¹⁰S. Schmitt-Rink, C. Ell, and H. Haug, Phys. Rev. B **33**, 1183 (1983).
- ¹¹M. S. Skolnick, J. M. Rorison, K. J. Nash, D. J. Mowbray, P. R. Tapster, S. J. Bass and A. D. Pitt, Phys. Rev. Lett. **58**, 2130 (1987).
- ¹²G. Livescu, D. A. B. Miller, D. S. Chemla, M. Ramaswamy, T. Y. Chang, N. Sauer, A. C. Gossard, and J. H. English, IEEE J. Quantum Electron. **QE-24**, 1677 (1988).
- ¹³J. S. Lee, Y. Iwasa, and N. Miura, Semicond. Sci. Technol. **2**, 675, (1987); J. Wagner, A. Ruiz, and K. Ploog, Phys. Rev. B **43**, No. 14, 12 134 (1991); J. Wagner, A. Fisher, and K. Ploog, Appl. Phys. Lett. **59**, 428 (1991); Yong-Hang Zhang, De-Sheng Jiang, R. Cingolani, and K. Ploog, *ibid.* **56**, 2195 (1990).
- ¹⁴W. Chen, M. Fritze, A. V. Nurmikko, J. M. Hong, and L. Chang, Phys. Rev. B **43**, 10 388, (1991).
- ¹⁵D. Heiman, B. B. Goldberg, A. Pinczuk, C. W. Tu, A. C. Gossard, and J. H. English, Phys. Rev. Lett. **61**, 605 (1988).
- ¹⁶S. K. Lyo Phys. Rev. B **40**, 8418 (1990); S. K. Lyo, E. D. Jones, and J. F. Klem, Phys. Rev. Lett. **61**, 2265 (1988).
- ¹⁷A. D. Wieck, F. Thiele, U. Merkt, K. Ploog, G. Weimann, and W. Schlapp, Phys. Rev. B **39**, 3785 (1989).
- ¹⁸C. Colvard, N. Nouri, H. Lee, and D. Ackley, Phys. Rev. B **39**, 8033 (1989).
- ¹⁹K. J. Nash, M. S. Skolnick, P. A. Claxton, and J. S. Roberts, Phys. Rev. B **39**, 5558 (1989).
- ²⁰G. E. W. Bauer and T. Ando, J. Phys. C **19**, 1553 (1986).
- ²¹G. Abstreiter, R. Merlin, and A. Piniczuk, IEEE J. Quantum Electron. **QE-22**, 1771 (1986).
- ²²J. F. Mueller, Phys. Rev. B **42**, 11 189 (1990).
- ²³T. Uenoyama and L. J. Sham, Phys. Rev. B **39**, 11 044 (1989).
- ²⁴P. E. Simmonds, T. A. Fisher, M. S. Skolnick, K. J. Nash, and R. S. Smith, *Proceedings of the Ninth International Conference on Electronic Properties of Two-Dimensional Systems, Nara, Japan* [Surf. Sci. (to be published)].
- ²⁵Glaucia M. G. Oliveira, Vivili M. S. Gomes, A. S. Chaves, J. R. Leite, and J. M. Worlock, Phys. Rev. B **35**, 2896 (1987).
- ²⁶U. Fano, Phys. Rev. **124**, 1866 (1961), J. J. Sakurai, *Modern Quantum Mechanics* (Benjamin-Cummings, Reading, MA, 1985), Chap. 5.
- ²⁷J. M. Calleja, A. R. Göni, B. S. Dennis, J. S. Weiner, A. Pinczuk, S. Schmitt-Rink, L. N. Pfeiffer, K. W. West, J. F. Muller, and A. E. Ruckenstein, Solid State Commun. **79**, 911 (1991).
- ²⁸T. Ando, A. Fowler, and F. Stern, Rev. Mod. Phys. **52**, 438 (1982).
- ²⁹M. Fritze, W. Chen, A. V. Nurmikko, J. Jo, M. Santos, and M. Shayegan, Phys. Rev. B **45**, 8408 (1992).
- ³⁰Ji-Wei Wu, Phys. Rev. B **40**, 8490 (1989).
- ³¹O. Akimoto and H. Hasegawa, J. Phys. Soc. Jpn. **22**, 181 (1966).